Supplementary Material

INVESTIGATING ULTRA-LOW VELOCITY ZONES IN THE SOUTHERN HEMISPHERE USING AN ANTARCTIC DATASET

Samantha E. Hansen[1], Sarah E. Carson[1], Edward J. Garnero[2], Sebastian Rost[3], and Shule Yu[2]

[1] Department of Geological Sciences, The University of Alabama

[2] School of Earth and Space Exploration, Arizona State University

[3] School of Earth and Environment, University of Leeds

Weighting Stacks

In Section 3.0, we describe the alignment and weighting scheme used to create the P and ScP stacks used for our ULVZ analysis. As noted, the individual waveforms are first aligned using the ScP and P predicted arrival times from the IASP91 reference model (Kennett and Engdahl, 1991), and linear stacks are generated. Each individual waveform is then cross-correlated with the linear stacks to determine an associated cross-correlation coefficient (CCC) and delay time. The individual waveforms are time-shifted by the correlated delay time to improve the alignment of the respective signal (*i.e.*, the P or ScP phase). The newly aligned waveforms are also weighted based on their signal-to-noise ratio (SNR) and associated CCC. Specifically, if the SNR is ≥ 50, the waveform is given full weight; if the SNR is between 40-49, it is weighted 0.75; if the SNR is between 20-39, it is weighted 0.50; if the SNR is between 10-19, it is weighted 0.25; otherwise, it is weighted 0.10. Similarly, if the CCC is ≥ 0.95, the waveform is weighted 1.50; if the CCC is between 0.85-0.94, it is weighted 1.20; if the CCC is between 0.75- 0.84, it is weighted 1.00; if the CCC is between 0.50-0.74, it is weighted 0.50; if the CCC is between 0.25-0.49, it is weighted 0.25; otherwise, it is weighted 0.10. The weights of both the SNR and CCC are combined to give a final weight for each station record. The aligned, weighted waveforms are then restacked to create a new stack for each phase, and this processes is repeated (as outlined in the main text) to create the final stacks for our analysis. Similar to Figure 3, Figure S1 provides additional examples of the individual ScP-waves recorded by the TAMNNET stations and their corresponding stacks, created with the scheme outlined above. It is worth noting that the maximum ScP CMB bounce point spread for these two events (02/01/2014 and 04/24/2015) are 109 and 112 km, respectively, and that despite this spread, they display coherent ScP waveforms across the array.

47 **Computing t* Operators and Event Ranking**

48 As also discussed in Section 3.0, each P-wave stack is convolved with a t* operator,
49 which represents the accumulated attenuation. The t* operator is defined by the following
50 (Equation 1), where *t* is the travel-time and *Q* is the quality factor (Futterman, 1962).

51 $$t^* = \int \frac{\mathrm{dt}}{\mathrm{Q}} \quad (1)$$

52 As noted in the main text, for each event, the P-wave stack is convolved with a series of t*
53 operators ranging from 0.10 to 2.30. The t*-convolved P-wave stacks are then compared to the
54 associated ScP stack by correlating their respective signals within a small time window centered
55 on the main ScP peak, where the signal amplitude is above zero (Fig. S2). The t* operator that
56 produces an attenuated P-wave response that most closely matches the associated ScP signal
57 within the examined time window is selected (Fig. S2).

58 As also noted in the main text, once the individual events were processed using the steps
59 outlined in Section 3.0, they were sorted into groups with A, B, or C rankings. Figure S3
60 provides examples of events meeting each of these ranking criteria. Further, Table S1
61 summarizes the t* applied to each A- and B-ranked event as well as their associated remainder
62 trace NRV, as defined in Section 4.0.

63 **Remainder Trace Standard Deviations**

64 In Section 4.0, we discuss how the remainder traces for each event were determined, and
65 we mention the associated standard deviation uncertainty. Also, in Section 5.0, we discuss the
66 various criteria each event was required to meet in order to be eligible for modeling, and one of
67 these criteria was that the ScP pre- and post-cursor energy in the remainder trace must exceed the
68 associated standard deviation. The standard deviation of the remainder trace (*d(remainder)*) was
69 computed using the following:

$$d(remainder) = \sqrt{\left(d(ScP))^2 + (d(P)\right)^2} \quad (2)$$

In Equation 2, *d(ScP)* and *d(P)* are the standard deviations of the ScP and P stacks, respectively, defined by the variation between the individual waveforms recorded at each station and the corresponding stack. As shown in Figure S4b, the remainder trace is plotted with its associated *d(remainder)*, which illustrates where the residual signal is larger than the associated uncertainty. In order for an event to be modeled, the pre- and/or post-cursor energy must extend past the standard deviations limits, as shown in this example. Across all examined events, the dominant pre- and post-cursor ScP energy above the standard deviation uncertainty fell within the residual signal window, described in Section 4.0.

Synthetic Seismograms

Also in Section 5.0, we discuss the range of synthetic models generated using the generalized ray method, which are ultimately compared to the observed ScP stacks. This comparison was performed over a 40 sec time window centered on the ScP peak (Fig. 7). The window size was chosen because it encompasses all possible ULVZ pre- and post-cursors from the range of examined models. This is illustrated by the examples shown in Figure S5. For progressively thicker ULVZs and/or progressively greater δV_P and δV_S reductions, the pre- and post-cursors can be seen moving out from the main ScP peak. We also note in Section 5.0 that the fit of the synthetics to the observations is assessed using the corresponding CCC, where a higher CCC (*i.e.*, closer to one) indicates a better model fit. While the computed CCC value does depend on the window length used for the comparison, we found that for our data, the same best-fit models were identified for the examined events even when a smaller window length was employed. This is illustrated in Figure S6, which shows plots comparable to those shown in

Figure 7; however, the window length used to assess model fit in this case is the same as that used to compute the remainder trace NRV, as described in Section 4.0 and as shown in Figure 4.

Supplemental Table and Figure Captions

Table S1. Event list with corresponding t* operators and NRV values. All A- and B-ranked events are summarized. Events are first sorted by rank, then by date.

Figure S1. Example ScP waveforms illustrating consistency across the array. Waveforms from event 02/01/2014 (top) and event 04/24/2015 (bottom), plotted in the same manner as panels (D) and (F) in Figure 3. Station names are indicated to the right of each trace with the corresponding stack shown below. Despite the spread in their ScP CMB bounce points, the events show coherent ScP signals across the array.

Figure S2. Example highlighting different attenuation (t^*) operators. The ScP stack (black) for the event shown in Figure 3 is compared to different attenuated P-wave stacks (red). The corresponding correlation is performed within a small window centered on the main ScP peak, where its amplitude is above zero (gray shaded region on top trace). Both the CCC and t^* values are listed to the right of each trace. The black box marks the best fit for this event. Note that in order to emphasize the signal, the time scale has been changed compared to Figure 3.

Figure S3. Examples of A-, B-, and C-ranked events. For each event, the attenuated P-wave stack is shown by the red trace, while the ScP stack is shown by the black trace.

Figure S4. Example showing standard deviation modeling criteria. (a) Example P-wave stack (red) plotted with its corresponding ScP stack (black). (b) Associated remainder trace (black) plotted with *d(remainder)* (gray shaded area). The red portions of the trace highlight where it extends past the uncertainty limits and thus shows significant signal.

Figure S5. Variability of synthetics. (a) Synthetic ScP waveforms resulting from models with progressively larger δV_P and δV_S, as indicated to the left of each trace. The ULVZ layer thickness (TH) was set to 40 km, and the $\delta\rho$ was set to 20%. The source was at a distance of 50°. Traces are aligned on their ScP arrivals, denoted by the bold gray vertical line. Thin gray lines denote the arrival times of the SdP and SPcP pre-cursors as well as the ScSP post-cursor, which are labeled below the bottom trace. (b) Same as (a) but in this case the models are associated with progressively thicker ULVZs while the δV_P and δV_S were set to -20% and -50%, respectively.

Figure S6. Synthetic modeling with smaller windows. Plotting is the same as Figure 7, but the comparison between the observed ScP stacks and the synthetic waveforms is now conducted over a time window that is the same as that used to compute the remainder trace NRV (Fig. 4). The computed CCC values vary with the window size, but the same best-fit models are identified, regardless of window size. The percent improvement in fit over a model without a ULVZ is comparable between Figures S6 and 7, again indicating that the data are better fit by a lowermost mantle having a ULVZ.

Table S1

Event Date	Latitude (°)	Longitude (°)	Depth (km)	Magnitude	Rank	t*	NRV
11/24/12	-21.47	-178.73	538.3	5.3	A	0.2	2.00
11/29/12	-20.80	-177.04	282.2	5.3	A	0.2	1.97
12/05/12	-31.14	-177.50	27.0	5.0	A	1.9	0.83
01/04/13	-29.65	-176.28	21.0	5.0	A	0.0	2.14
02/12/13	-18.22	-177.85	524.7	5.6	A	0.8	1.85
02/16/13	-36.23	178.03	198.4	5.8	A	1.2	2.92
04/26/13	-28.73	-178.90	355.4	6.2	A	0.2	3.89
06/15/13	-33.90	179.49	210.0	6.0	A	0.0	2.03
07/29/13	-57.86	-25.40	41.1	5.2	A	1.4	2.58
09/09/13	-14.69	167.34	151.9	5.0	A	2.2	2.42
11/03/13	-57.87	-25.66	45.9	5.3	A	1.5	2.09
11/23/13	-17.16	-176.52	370.1	6.5	A	0.0	2.06
12/04/13	-25.47	178.35	585.8	5.8	A	0.0	7.78
12/15/13	-17.20	168.47	200.0	5.0	A	1.2	1.68
12/17/13	-20.75	-178.67	602.2	5.7	A	0.8	1.61
02/01/14	-56.83	-27.34	130.0	6.1	A	0.0	3.10
07/03/14	-30.46	-176.45	35.0	6.3	A	0.8	1.09
04/28/15	-20.89	-178.63	581.0	6.1	A	0.7	1.49
06/20/15	-59.63	-26.50	50.1	5.7	A	0.8	2.62
06/21/15	-20.43	-178.33	562.6	6.0	A	1.4	3.81
09/07/15	-24.24	179.13	535.0	6.0	A	0.3	4.31
11/29/12	-21.21	-178.62	550.9	5.5	B	0.9	1.08
11/29/12	-28.49	-178.28	252.6	5.5	B	0.0	2.13
11/30/12	-18.96	-175.51	202.8	5.6	B	1.5	1.57
12/05/12	-31.14	-177.50	27.0	5.0	B	1.9	0.61
12/21/12	-20.85	-173.85	34.7	5.0	B	1.0	1.35
12/30/12	-60.92	-36.92	10.0	5.0	B	1.0	0.64
02/19/13	-17.62	-173.38	42.2	5.7	B	0.0	1.17
02/26/13	-21.45	-179.28	603.5	5.8	B	1.8	1.28
03/12/13	-55.50	-27.75	10.0	5.1	B	2.1	0.68
04/05/13	-31.86	-177.62	18.0	5.1	B	0.5	1.26
04/06/13	-19.61	-174.92	104.2	5.2	B	1.9	1.14
04/13/13	-19.10	169.65	269.3	6.0	B	1.7	1.75
04/22/13	-29.91	-176.10	10.8	5.3	B	2.3	0.91

05/15/13	-27.30	-177.91	180.0	5.2	B	0.6	3.78
05/16/13	-22.23	-179.51	596.3	5.3	B	1.0	2.65
06/05/13	-23.45	-179.75	564.3	5.2	B	0.1	6.40
06/07/13	-43.85	-16.30	10.0	5.7	B	2.0	1.10
07/16/13	-60.03	-26.35	26.0	5.0	B	1.1	1.71
07/26/13	-20.75	-174.71	45.0	5.3	B	1.8	0.97
08/08/13	-20.35	-176.41	249.7	5.5	B	1.0	2.98
08/16/13	-41.73	174.30	13.4	5.3	B	0.7	3.30
08/28/13	-27.79	179.75	485.1	6.2	B	1.5	1.74
08/29/13	-19.40	-179.02	674.3	5.8	B	1.1	1.78
09/30/13	-30.88	-178.25	37.8	6.4	B	0.8	2.81
10/03/13	-29.64	-178.38	188.6	5.2	B	0.0	2.97
10/15/13	-15.23	167.56	133.0	5.3	B	0.9	1.60
10/23/13	-22.97	-177.04	157.7	6.0	B	0.0	1.95
10/28/13	-56.28	-27.37	114.4	5.0	B	0.6	1.72
10/29/13	-20.06	-178.23	580.2	5.1	B	2.0	5.69
11/01/13	-20.85	-178.47	549.5	5.5	B	0.2	3.59
11/02/13	-11.80	166.77	219.7	5.0	B	2.1	1.97
11/03/13	-19.49	-172.55	12.5	5.5	B	0.8	0.45
11/18/13	-60.53	-43.45	11.3	5.2	B	1.2	0.94
11/22/13	-57.79	-25.30	10.0	5.2	B	1.4	0.98
12/01/13	-17.57	-178.26	534.8	5.7	B	0.9	0.97
12/02/13	-21.25	170.26	125.2	5.7	B	0.9	2.91
02/02/14	-32.91	-177.88	44.3	6.5	B	1.1	1.41
03/11/14	-60.86	-19.98	10.0	6.4	B	1.0	0.76
04/26/14	-20.75	-174.71	45.0	6.1	B	2.0	0.90
05/01/14	-21.45	170.35	106.0	6.6	B	1.1	3.28
08/27/14	-15.05	167.39	115.3	5.9	B	0.2	1.27
11/01/14	-19.69	-177.76	434.0	7.1	B	1.7	1.85
01/28/15	-20.97	-178.30	484.1	6.2	B	0.8	2.13
04/24/15	-42.06	173.01	48.0	6.1	B	2.0	5.90
05/24/15	-59.65	-26.45	34.0	5.8	B	0.6	1.37
07/07/15	-22.94	-177.13	169.6	5.8	B	2.1	1.14
07/29/15	-25.37	154.23	9.0	5.5	B	1.4	1.00
09/30/15	-56.19	-27.72	101.0	5.7	B	0.5	1.51
10/20/15	-14.86	167.30	135.0	7.1	B	1.4	1.81
10/25/15	-29.33	-177.80	10.0	5.8	B	0.0	0.87

Event 02/01/2014

Max ScP CMB bounce point spread: 109 km

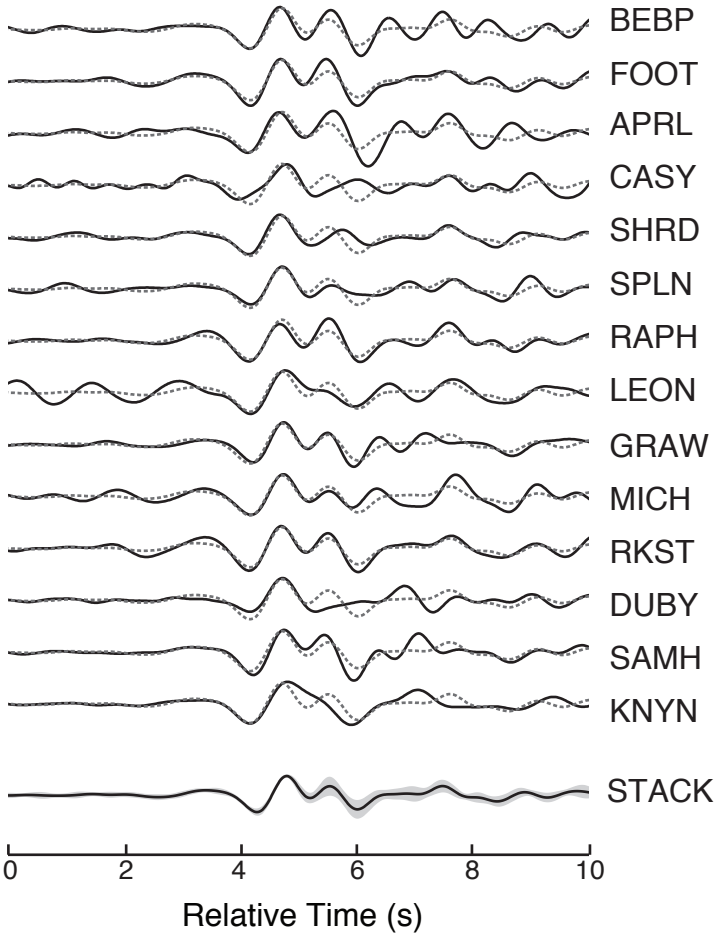

Event 04/24/2015

Max ScP CMB bounce point spread: 112 km

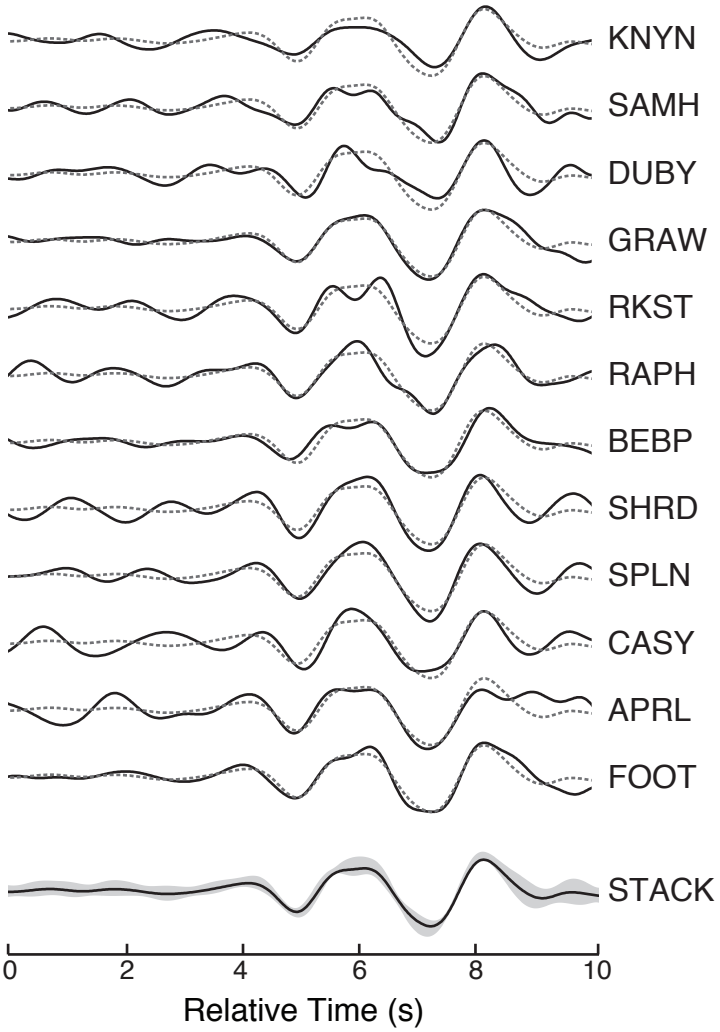

Figure S1

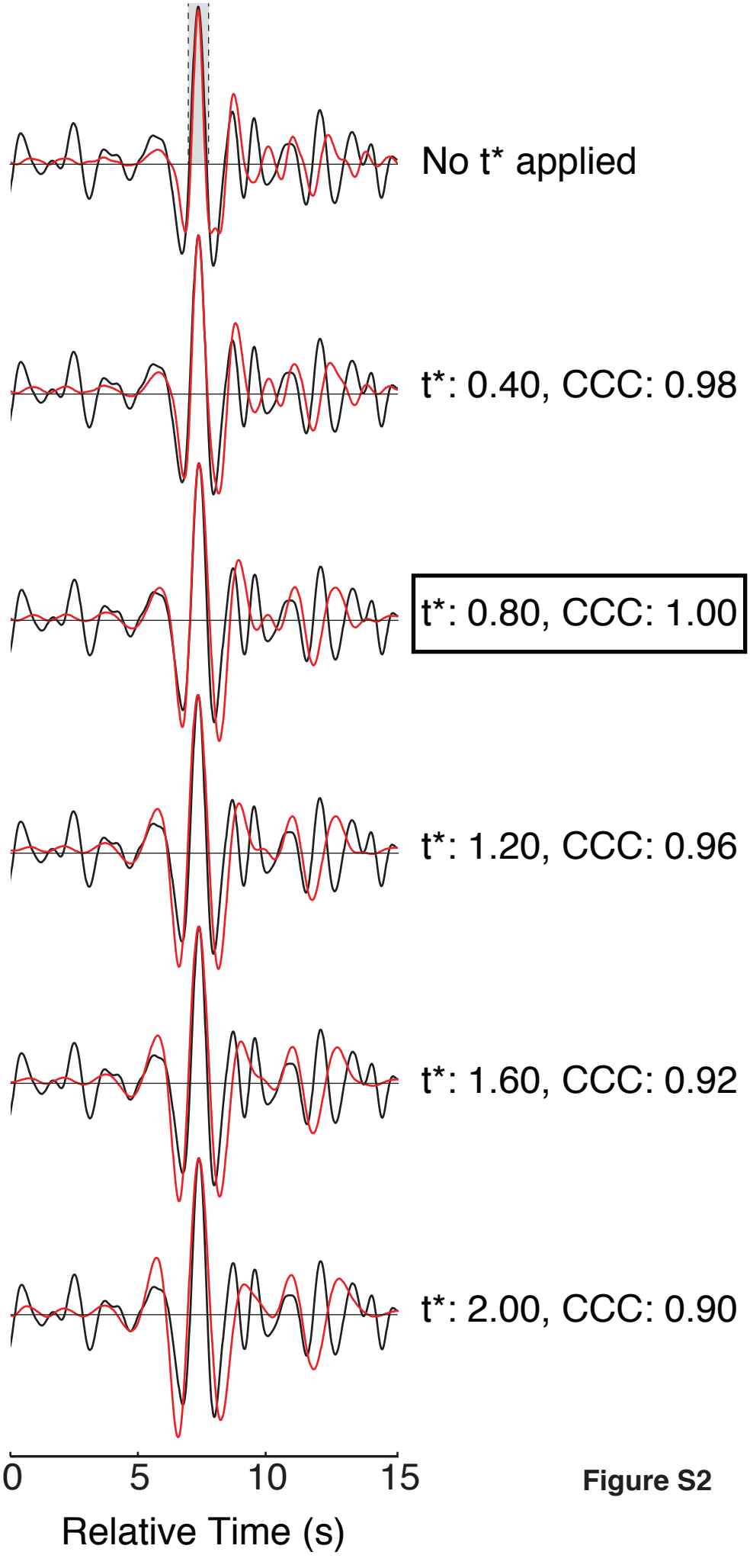
No t* applied
t*: 0.40, CCC: 0.98
t*: 0.80, CCC: 1.00
t*: 1.20, CCC: 0.96
t*: 1.60, CCC: 0.92
t*: 2.00, CCC: 0.90
0
5
10
15
Relative Time (s)

Figure S2

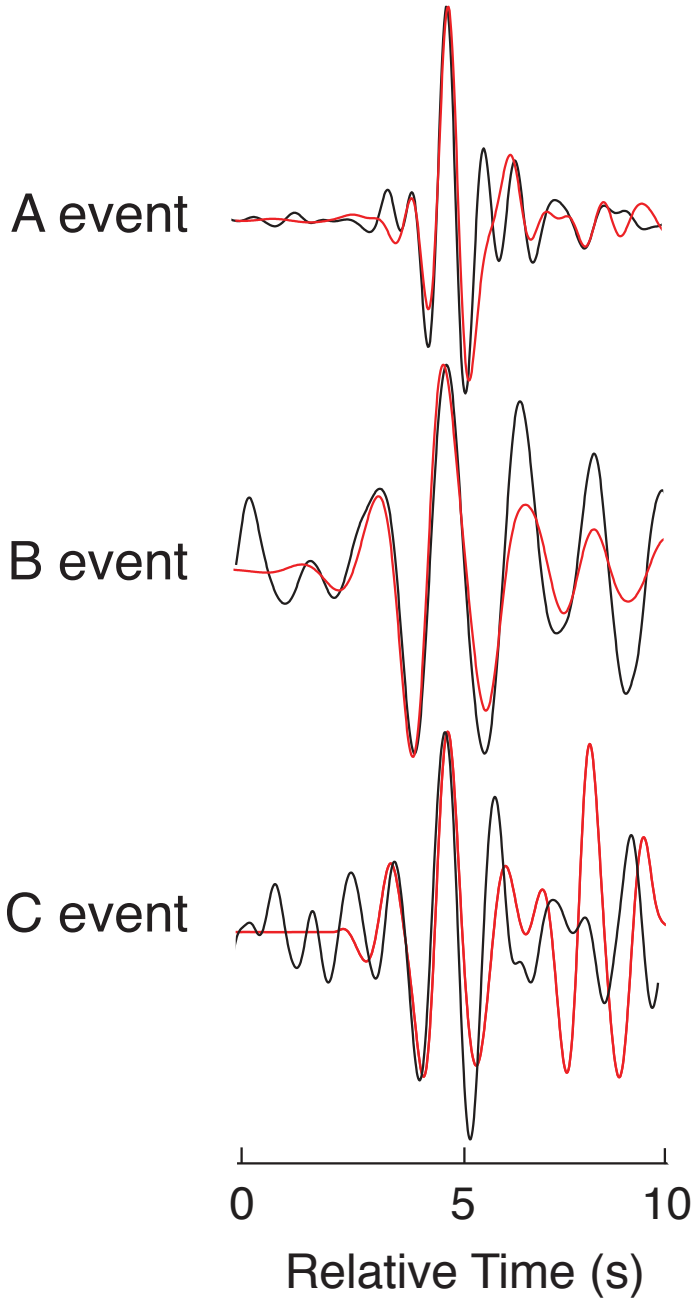

Figure S3

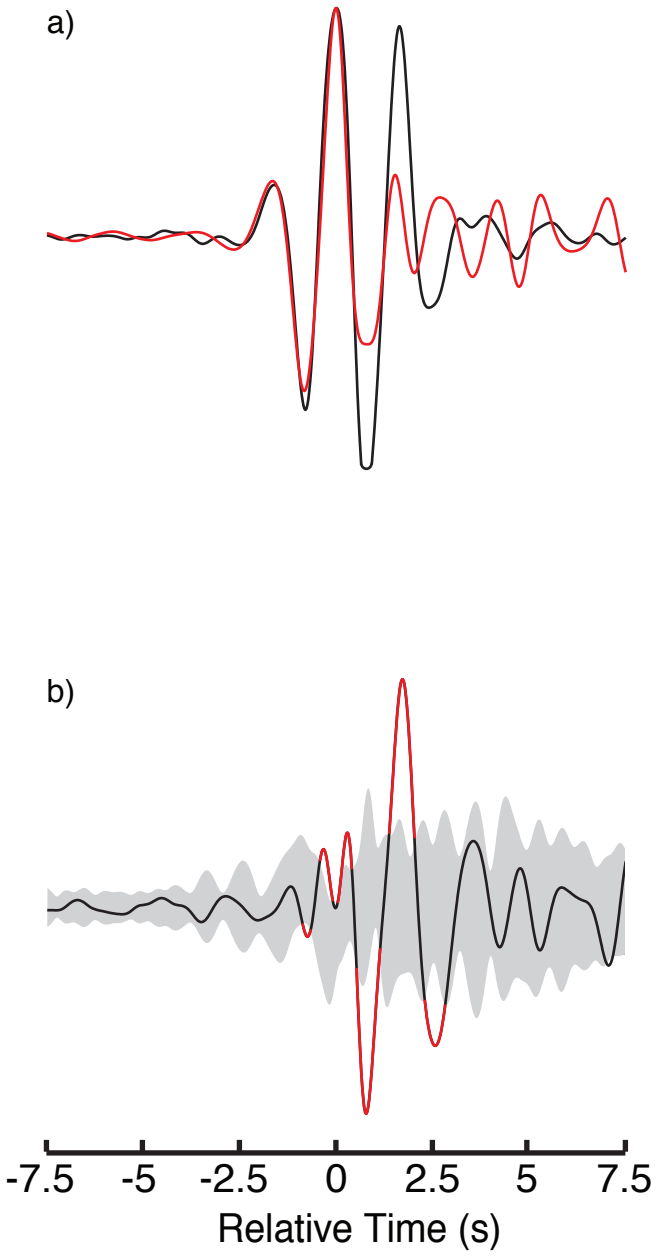

Figure S4

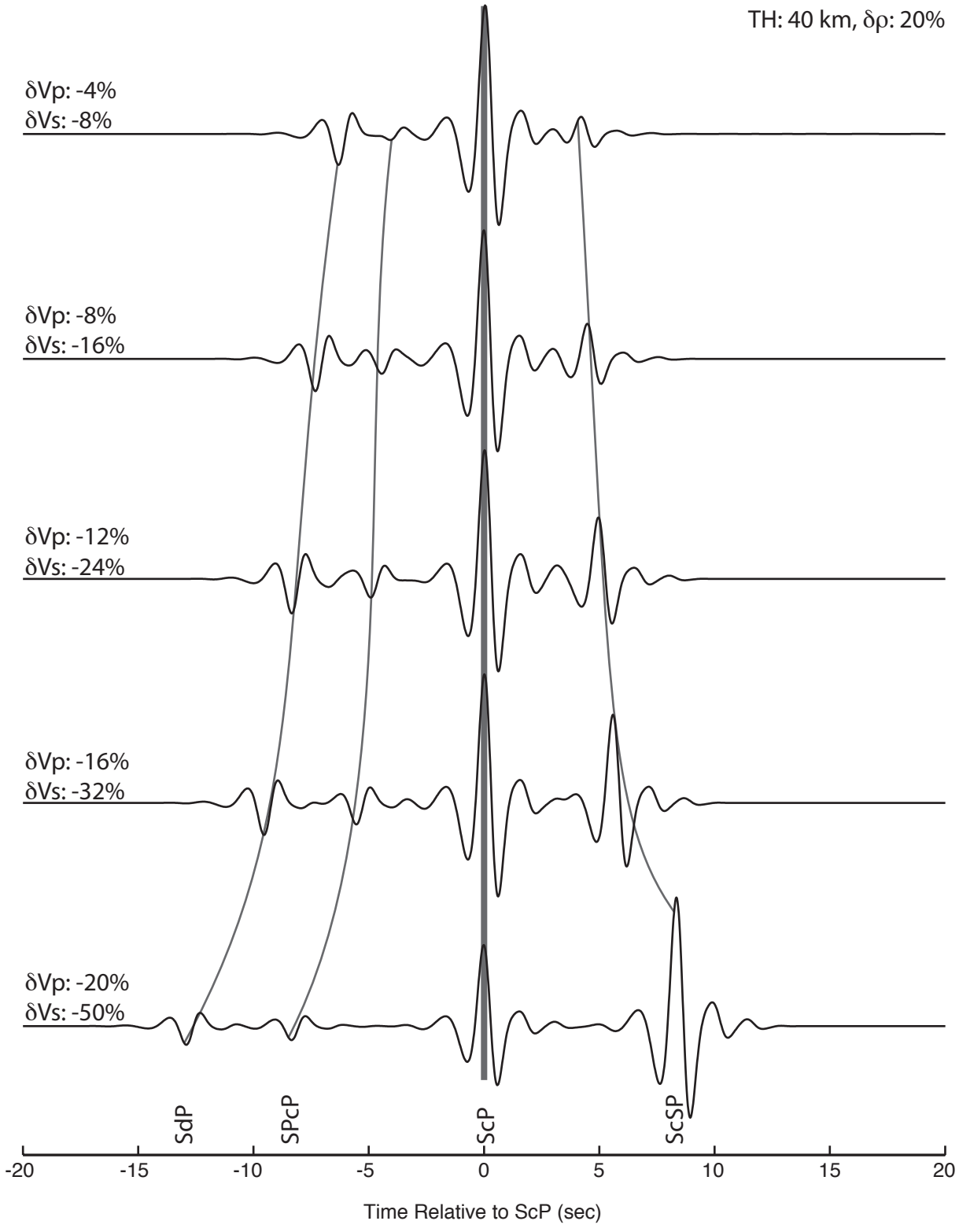
TH: 40 km, δρ: 20%
δVp: -4%
δVs: -8%
δVp: -8%
δVs: -16%
δVp: -12%
δVs: -24%
δVp: -16%
δVs: -32%
δVp: -20%
δVs: -50%
SdP
SPcP
ScP
ScSP
-20
-15
-10
-5
0
5
10
15
20
Time Relative to ScP (sec)

Figure S5a

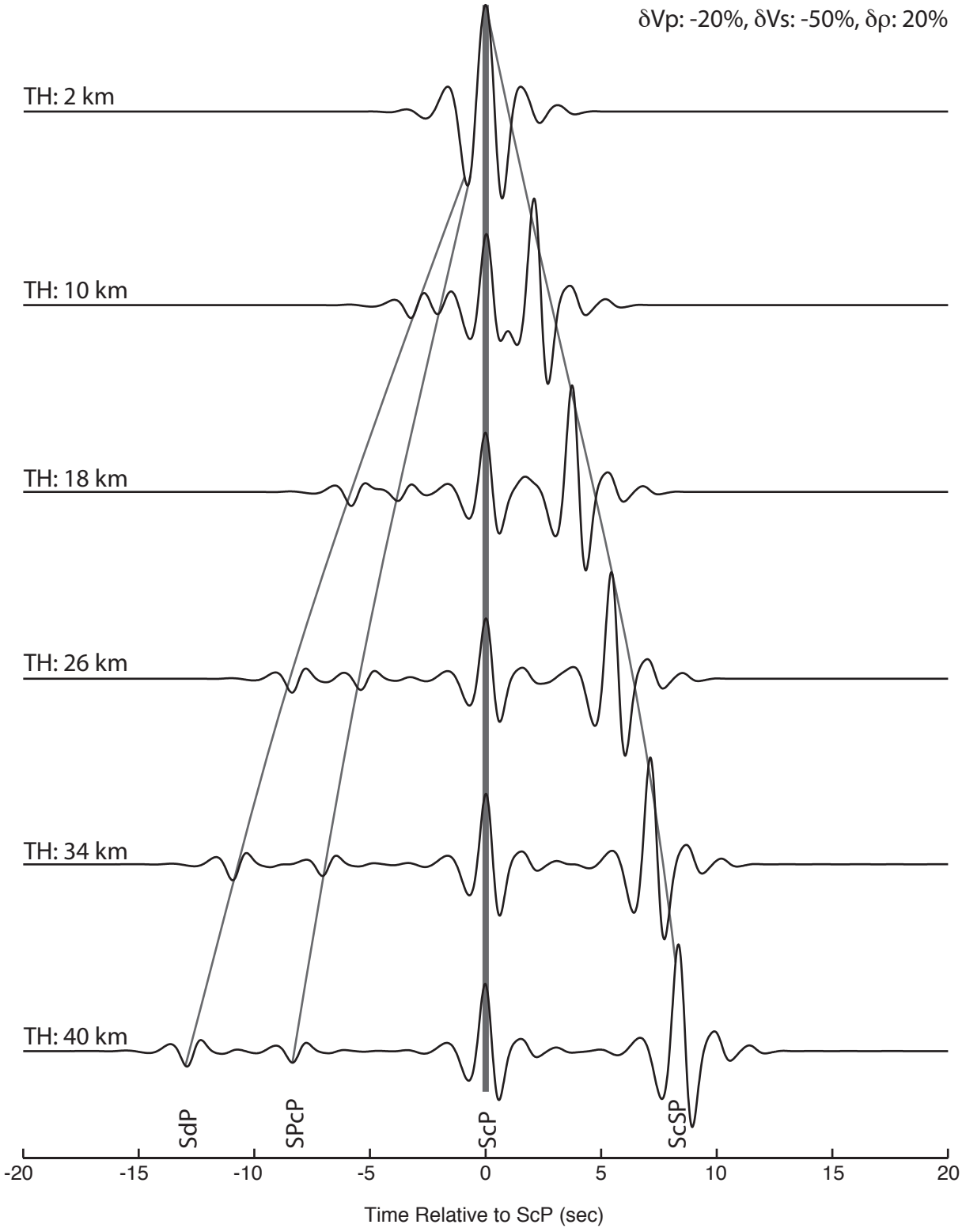
δVp: -20%, δVs: -50%, δρ: 20%
TH: 2 km
TH: 10 km
TH: 18 km
TH: 26 km
TH: 34 km
TH: 40 km
SdP
SPcP
ScP
ScSP
-20
-15
-10
-5
0
5
10
15
20
Time Relative to ScP (sec)

Figure S5b

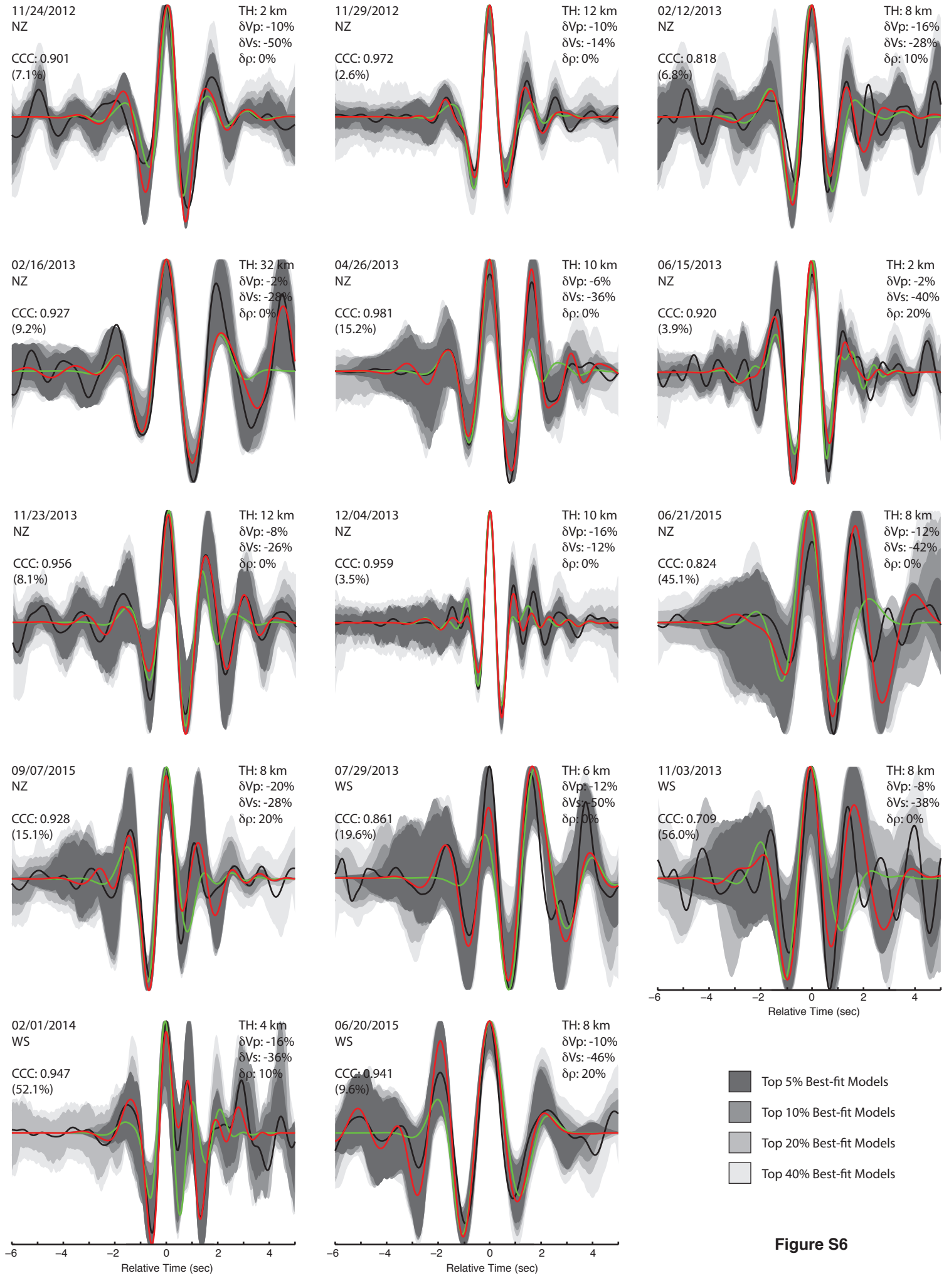
11/24/2012
NZ
CCC: 0.901
(7.1%)
TH: 2 km
δVp: -10%
δVs: -50%
δρ: 0%
11/29/2012
NZ
CCC: 0.972
(2.6%)
TH: 12 km
δVp: -10%
δVs: -14%
δρ: 0%
02/12/2013
NZ
CCC: 0.818
(6.8%)
TH: 8 km
δVp: -16%
δVs: -28%
δρ: 10%
02/16/2013
NZ
CCC: 0.927
(9.2%)
TH: 32 km
δVp: -2%
δVs: -28%
δρ: 0%
04/26/2013
NZ
CCC: 0.981
(15.2%)
TH: 10 km
δVp: -6%
δVs: -36%
δρ: 0%
06/15/2013
NZ
CCC: 0.920
(3.9%)
TH: 2 km
δVp: -2%
δVs: -40%
δρ: 20%
11/23/2013
NZ
CCC: 0.956
(8.1%)
TH: 12 km
δVp: -8%
δVs: -26%
δρ: 0%
12/04/2013
NZ
CCC: 0.959
(3.5%)
TH: 10 km
δVp: -16%
δVs: -12%
δρ: 0%
06/21/2015
NZ
CCC: 0.824
(45.1%)
TH: 8 km
δVp: -12%
δVs: -42%
δρ: 0%
09/07/2015
NZ
CCC: 0.928
(15.1%)
TH: 8 km
δVp: -20%
δVs: -28%
δρ: 20%
07/29/2013
WS
CCC: 0.861
(19.6%)
TH: 6 km
δVp: -12%
δVs: -50%
δρ: 0%
11/03/2013
WS
CCC: 0.709
(56.0%)
TH: 8 km
δVp: -8%
δVs: -38%
δρ: 0%
−6
−4
−2
0
2
4
Relative Time (sec)
02/01/2014
WS
CCC: 0.947
(52.1%)
TH: 4 km
δVp: -16%
δVs: -36%
δρ: 10%
06/20/2015
WS
CCC: 0.941
(9.6%)
TH: 8 km
δVp: -10%
δVs: -46%
δρ: 20%
−6
−4
−2
0
2
4
Relative Time (sec)
Top 5% Best-fit Models
Top 10% Best-fit Models
Top 20% Best-fit Models
Top 40% Best-fit Models

Figure S6